International Journal of Biological Macromolecules 269 (2024) 131840

Contents lists available at ScienceDirect

International Journal of Biological Macromolecules

journal homepage: www.elsevier.com/locate/ijbiomac

Investigation of the MDM2-binding potential of *de novo* designed peptides using enhanced sampling simulations

Olanrewaju Ayodeji Durojaye [a,b,c,**,1], Abeeb Abiodun Yekeen [d,e,1], Mukhtar Oluwaseun Idris [f], Nkwachukwu Oziamara Okoro [g], Arome Solomon Odiba [h,i,*], Bennett Chima Nwanguma [h,i,*]

[a] MOE Key Laboratory of Membraneless Organelle and Cellular Dynamics, Hefei National Laboratory for Physical Sciences at the Microscale, University of Science and Technology of China, Hefei, Anhui 230027, China
[b] School of Life Sciences, University of Science and Technology of China, Hefei, Anhui 230027, China
[c] Department of Chemical Sciences, Coal City University, Emene, Enugu State, Nigeria
[d] Department of Radiation Oncology, University of Texas Southwestern Medical Center, Dallas, TX 75390, United States
[e] Department of Biochemistry, University of Texas Southwestern Medical Center, Dallas, TX 75390, United States
[f] Biochemistry and Biophysics Department, Oregon State University, Corvallis, United States
[g] Department of Pharmaceutical and Medicinal Chemistry, Faculty of Pharmaceutical Sciences, University of Nigeria, Nsukka 410001, Nigeria
[h] Department of Molecular Genetics and Biotechnology, University of Nigeria, Nsukka, Enugu State 410001, Nigeria
[i] Department of Biochemistry, Faculty of Biological Sciences, University of Nigeria, Nsukka, Enugu State 410001, Nigeria

ARTICLE INFO

Keywords:
MDM2
p53
Protein design
Enhanced sampling simulation
Peptide binder

ABSTRACT

The tumor suppressor p53 plays a crucial role in cellular responses to various stresses, regulating key processes such as apoptosis, senescence, and DNA repair. Dysfunctional p53, prevalent in approximately 50 % of human cancers, contributes to tumor development and resistance to treatment. This study employed deep learning-based protein design and structure prediction methods to identify novel high-affinity peptide binders (Pep1 and Pep2) targeting MDM2, with the aim of disrupting its interaction with p53. Extensive all-atom molecular dynamics simulations highlighted the stability of the designed peptide in complex with the target, supported by several structural analyses, including RMSD, RMSF, Rg, SASA, PCA, and free energy landscapes. Using the steered molecular dynamics and umbrella sampling simulations, we elucidate the dissociation dynamics of p53, Pep1, and Pep2 from MDM2. Notable differences in interaction profiles were observed, emphasizing the distinct dissociation patterns of each peptide. In conclusion, the results of our umbrella sampling simulations suggest Pep1 as a higher-affinity MDM2 binder compared to p53 and Pep2, positioning it as a potential inhibitor of the MDM2-p53 interaction. Using state-of-the-art protein design tools and advanced MD simulations, this study provides a comprehensive framework for rational *in silico* design of peptide binders with therapeutic implications in disrupting MDM2-p53 interactions for anticancer interventions.

1. Introduction

Rational drug design, a prevalent strategy in the drug discovery process, often employs computational tools, such as the docking of virtual libraries, to design small molecules with therapeutic potential [1–4]. While these tools have proven effective for small molecules, they encounter limitations when applied to the design of peptides [5–8]. Peptides, known for their intrinsic disorder and the propensity to adopt stable structures only in the presence of binding partners, pose a unique challenge for traditional computational approaches [9,10]. Contrary to the rigid structures typically targeted by small molecules, peptide molecules exhibit flexibility and a complementary nature to proteins, offering a distinct advantage [11,12]. This flexibility allows peptide inhibitors to interact with proteins categorized as "undruggable" by small molecules, broadening the scope of potential drug targets. The adaptability of peptides makes them particularly well-suited for binding

* Corresponding authors at: Department of Molecular Genetics and Biotechnology, University of Nigeria, Nsukka, Enugu State 410001, Nigeria.
** Correspondence to: O. A. Durojaye, MOE Key Laboratory of Membraneless Organelle and Cellular Dynamics, Hefei National Laboratory for Physical Sciences at the Microscale, University of Science and Technology of China, Hefei, Anhui 230027, China.
E-mail addresses: lanredurojaye@mail.ustc.edu.cn (O.A. Durojaye), arome.odiba@unn.edu.ng (A.S. Odiba), bennett.nwanguma@unn.edu.ng (B.C. Nwanguma).
[1] These authors contributed equally to this work.

https://doi.org/10.1016/j.ijbiomac.2024.131840
Received 14 February 2024; Received in revised form 13 April 2024; Accepted 22 April 2024
Available online 26 April 2024

to dynamic and challenging protein surfaces [13].

In recent advancements, *de novo* protein design has emerged as a transformative approach, enabling the creation of peptides with remarkable binding affinity and specificity for structured proteins [14]. This method opens up new avenues for designing therapeutic agents that can precisely target proteins implicated in various diseases, even those previously considered difficult to drug [15]. The ability to harness the flexibility and adaptability of peptides through innovative design strategies marks a significant stride in expanding the repertoire of drug discovery tools and holds promise for developing highly selective and effective therapeutics [16].

The tumor suppressor p53 protein plays a pivotal role in cellular responses to various stresses, such as DNA damage or oncogene activation. Upon activation, p53 transcriptionally regulates a multitude of target genes that orchestrate important cellular processes including apoptosis, senescence, repair of the DNA, and arrest of the cell-cycle [17,18]. These responses collectively aim to impede the proliferation of damaged cells, mitigating the risk of passing mutations to subsequent generations [19,20]. Notably, in approximately 50 % of human cancers, p53 functionality is compromised, primarily due to somatic mutations or deletions in its DNA-binding domain. Posttranslational modifications, such as methylation, phosphorylation, and acetylation, further contribute to p53 dysfunction and instability [21,22]. The altered p53 fails to effectively regulate crucial cellular responses to DNA damage, directly contributing to tumor development, malignant progression, poor prognosis, and resistance to treatment [23]. Conversely, reinstating endogenous p53 activity holds immense therapeutic potential. Restoration of functional p53 can halt the growth of cancerous tumors *in vivo* by inducing apoptosis, senescence, and innate inflammatory responses [23,24].

The MDM2 oncoprotein serves as a potent cellular inhibitor of the p53 tumor suppressor by engaging in a molecular interaction with the transactivation domain of p53, consequently diminishing its capacity to activate transcription [25]. This inhibitory mechanism employed by MDM2 plays a pivotal role in the downregulation of p53 function. Notably, in specific cancer types, the phenomenon of MDM2 amplification emerges as a recurrent and widespread event [25]. This amplification of MDM2 significantly contributes to the inactivation of p53, exacerbating the suppression of p53-mediated transcriptional activity. In essence, the dysregulation of the MDM2-p53 axis, often fueled by MDM2 amplification, represents a critical molecular aberration implicated in certain cancers, where the compromised functionality of p53 facilitates the progression and survival of malignant cells [25]. In the context of this study, our approach involved leveraging deep learning-based protein design methods, coupled with all-atom and enhanced sampling molecular dynamics (MD) simulations facilitated by our previously reported automation tool for GROMACS-based MD simulation called CHAPERONg [26]. Deep learning refers to a subset of machine learning techniques that involve training artificial neural networks with multiple layers to analyze and interpret complex data [27]. Advanced deep learning-based techniques have been employed to enhance pre-existing energy-based theoretical frameworks in computational protein design, starting from scratch (*de novo*) [28]. This has led to a remarkable tenfold surge in the efficacy rates, as corroborated through experimental validation, for the successful binding of a custom-designed protein with its intended target protein [28]. Our overarching objective is to identify potential high-affinity peptide binders targeting MDM2, with the ultimate aim of disrupting its interaction with p53. This strategy integrates cutting-edge computational methodologies to design peptides that hold promise for therapeutic interventions aimed at restoring the crucial tumor-suppressive functions of p53 and combating cancer progression.

2. Methods

2.1. Peptide design workflow

The peptide design workflow employed for generating high-affinity peptide binders targeting MDM2 was initiated with the acquisition of a high-quality structure of the MDM2-p53 protein-peptide complex from the Protein Data Bank (PDB: 1YCR). This complex structure served as the input structure for the first phase of our design strategy. We generated *de novo* peptide backbones targeted at the p53-binding interface of the MDM2 receptor using the RFdiffusion program [28] implemented on the Tamarind bio platform [29]. Eight diffused designs, each of 13–15 residues, were generated through two distinct runs to facilitate variability in the backbone conformations of the peptides.

The resultant library of diverse peptide backbones underwent sequence design using ProteinMPNN [30], leveraging its capabilities to optimize amino acid sequences based on structural and functional considerations. AlphaFold-Multimer [31–33] was employed to refine and filter the designed sequences using its confidence metrics including the predicted Local Distance Difference Test (pLDDT), predicted Aligned Error (PAE), and predicted Template Modeling (pTM scores), as well as the structural agreement between the designed models and AlphaFold-Multimer complex predictions based on root mean square deviation (RMSD). Additional validations were further carried out on the predicted models using DMFold [34].

2.2. Surface electrostatic potential and thermal stability predictions

To assess the electrostatic potential within the individual components of protein-peptide complexes, the APBS electrostatics plugin in PyMOL was employed [35]. For the prediction of thermal stability for each peptide, we employed the deep learning-based DeepSTABp tool [27]. The FASTA sequences of each peptide were provided as input to DeepSTABp, with the growth temperature set to the default value of 22 °C. For each prediction, the calculations were conducted for both cellular and lysate environments.

2.3. All-atom molecular dynamics simulations

The all-atom MD simulations conducted for our protein-peptide complexes of interest were extended to a production time of 1 microsecond each. These simulations were executed using the GROMACS (GROningen MAchine for Chemical Simulations) software, version 2020 [36]. Prior to running the simulations, the residues in the AlphaFold-Multimer-predicted complexes were renumbered to be consistent with the numbering of the p53-MDM2 complex using the UCSF Chimera software [37]. The CHARMM36 force field [38] was chosen to parameterize the systems. To create a physiologically relevant environment, the systems were solvated in cubic boxes using 4-point TIP3P water molecules placed at a minimum distance of 1.0 nm from the simulation box edge. To achieve system neutrality, Cl^- and Na^+ ions were introduced, maintaining a physiological salt concentration conducive to realistic molecular environments. The solvated systems underwent energy minimization comprising 5000 steps, and employing the steepest descent algorithm for structural relaxation. Equilibration followed, involving 100 ps of NVT ensembles at 1 atm pressure and 300 K, implemented through the Nose-Hoover scheme with a coupling constant of 1.0 ps and an isotropic Parrinello-Rahman barostat [39,40]. Throughout the simulations, the PME (Particle Mesh Ewald) method was employed for long-range electrostatic interactions [41]. To maintain the integrity of covalent bonds involving hydrogen atoms, the LINCS algorithm was employed, effectively constraining their movements [42]. A notable aspect of our methodology involves the utilization of our recently developed automation tool, CHAPERONg [26], for GROMACS-based MD simulations and analyses. This tool streamlines the entire simulation process, enhancing efficiency and reproducibility in

trajectory analyses. Trajectory plots derived from the simulations were visualized using XMGRACE [43].

2.4. Steered molecular dynamics simulations

For each run per protein-peptide complex, the steered molecular dynamics (SMD) simulations were executed over a duration of 500 ps with a spring force constant set at 1000 kJ $mol^{-1} nm^{-2}$. A constant harmonic pulling rate of 10 nm per nanosecond was employed in the y-direction resulting in a pull distance of 5 nm. During the pulling simulations, the center of mass of each peptide, namely p53, Pep1, and Pep2, was pulled along the y-direction (the reaction coordinate) while a position restraint was applied on MDM2 to confine it to its specified position. Each SMD simulation was conducted in three independent replica runs, and for each run, per-picosecond snapshots of the trajectory were recorded.

2.5. Umbrella sampling simulations

Following the completion of the SMD simulations, the subsequent phase involved conducting umbrella sampling computations. Using a center of mass spacing of 0.2 nm along the reaction coordinates, the starting configurations for the umbrella sampling were selected from the SMD trajectory snapshots. To ensure a comprehensive exploration of the reaction landscape, particularly in cases necessitating additional sampling, supplementary windows were systematically generated. This deliberate expansion of sampling windows not only served to create a statistically significant potential mean force variation but also played a crucial role in confirming the adequacy and appropriateness of the selected sampling windows along the reaction coordinates.

For each of the designed sampling windows, a 100-picosecond NPT (constant Number of particles, Pressure, and Temperature) equilibration phase was initiated. Following this equilibration, a 4-nanosecond umbrella sampling simulation ensued, accumulating to a total MD simulation time of 104 ns for the MDM2-p53 complex and 107 ns for each of the complexes involving MDM2 with Pep1 and Pep2. Throughout these simulations, the Parinello-Rahman type barostat was employed (as described in the all-atom MD simulations) to maintain a constant pressure [40], and the Nose-Hoover thermostat [39] for temperature control. Similar to the SMD, each umbrella sampling simulation was conducted in three independent replica runs.

The trajectory data from the simulations was subjected to analysis using the Weighted Histogram Analysis Method [44] to calculate the binding free energy ($\Delta G_{binding}$) between MDM2 and its respective peptides—p53, Pep1, and Pep2.

3. Results and discussion

3.1. De novo design of peptide binders to strategically target the MDM2-p53 interface

To design peptide binders capable of competitively engaging with the interface binding pocket of MDM2 against p53, we utilized Rfdiffusion, a generative model of protein backbones that exhibits exceptional performance in designing peptide binders [45]. We strategically selected a subset of hotspot residues on the target MDM2 receptor to guide the RFdiffusion process. To identify these crucial hotspots, we conducted an in-depth analysis of the interaction interface between the MDM2-p53 complex (PDB: 1YCR). The MDM2 cleft revealed 14 conserved hydrophobic and aromatic amino acids forming multiple van der Waals contacts with p53 [25]. The positioning of the p53 helix facilitates the insertion of Phe19, Trp23, and Leu26 along its hydrophobic face into the MDM2 cleft, creating a complementary packing arrangement. Notably, the closest contact at the interface occurs between Phe19 and Trp23 of p53 and the body of the α2 helix of MDM2. Phe19 establishes van der Waals contacts with Ile61 and Gly58 of MDM2, while Trp23 forms similar interactions with the same set of MDM2 residues (Gly58 and Ile61) [25]. Based on this analysis, we identified Ile61 and Gly58 of MDM2 as essential hotspot residues fed to RFdiffusion to guide the diffusion process toward generating peptide backbones with optimal binding potential at the MDM2 interface.

The protein sequence design challenge involves the identification of amino acid sequences that, when folded, correspond to given protein backbone structures. Having employed RFdiffusion to generate backbone models, we leveraged the deep learning-based protein sequence design approach of ProteinMPNN [30]. By providing the generated backbone models as input, ProteinMPNN designs different sets of amino acid sequences for the provided backbone structures. These sets of amino acid sequences were subsequently employed as input for 3D structure prediction with AlphaFold-Multimer for evaluation using its various confidence measures, including ipTM, pTM, PAE, and pLDDT [33]. It is essential to consider these measures to assess the accuracy and confidence of the predicted protein structures. While pLDDT is a valuable local measure, it may not be sensitive to the spatial arrangement of individual domains in multi-domain proteins. Consequently, a high pLDDT score may not guarantee overall high confidence in the entire protein structure. In instances involving proteins with multiple domains, a scenario with a high pLDDT and a low pTM score could indicate accurate prediction of individual domains but insufficient confidence in their relative orientation.

Our ultimate criterion for the selection of peptides for the next steps was the agreement of the designed structural model with the AlphaFold-Multimer prediction of the complex. For this, the designed model for each MDM2-peptide complex was structurally aligned with its AlphaFold-Multimer prediction and the RMSD was calculated. From the diverse pool of predicted sequences, we selected two peptide candidates (MLKEALEELAEWAE and GFELLEEVWQEVLEK) with not only the lowest RMSD values of 2.36 and 1.43 respectively (Fig. 1A–C), but also acceptable pLDDT and PAE scores (Fig. 1D–G).

To validate our predictions, we subjected the designed complexes of interest—MDM2 in complex with MLKEALEELAEWAE (now designated as Pep1) and GFELLEEVWQEVLEK (now designated as Pep2)—to analysis using an alternate structure prediction tool, DMFold (Supplementary Fig. S1). Superimposition of the DMFold-predicted complexes onto the earlier predicted structures with AlphaFold multimer provided additional layers of confidence in our prediction outputs (although, with a low accuracy pLDDT prediction for Pep2) (Supplementary Fig. S1). This dual-method approach enhanced the robustness and credibility of our findings, reinforcing the accuracy and reliability of the structural predictions for the peptide binders (Pep1 and Pep2) in complex with MDM2.

3.2. Electrostatic complementarity of the designed peptides suggests strong binding potential

Given the pivotal roles of electrostatic interactions in various biological phenomena, including molecular recognition, protein solubility, viscosity, protein–protein interactions, and protein stability [46–49], our study aimed to systematically quantify and characterize the electrostatic properties of the reference peptides. This exploration sought to enhance our understanding of their binding potentials to MDM2 through electrostatic complementarity.

To perform a detailed analysis of the surface electrostatic potential, we used the experimentally derived 3D structure of the MDM2-p53 complex (PDB accession code: 1YCR) and the Alphafold multimer-predicted structures of Pep1 and Pep2 in complex with MDM2. The electrostatic potential calculations were executed with each peptide separated from MDM2, the common interacting partner. The comparative assessment of the resultant data, as depicted in Fig. 1G, revealed an augmented negative electrostatic potential in specific regions of Pep1 and Pep2 (in contrast to p53) that exhibited complementarity to the positive potential of the MDM2 binding site. This observation suggests a

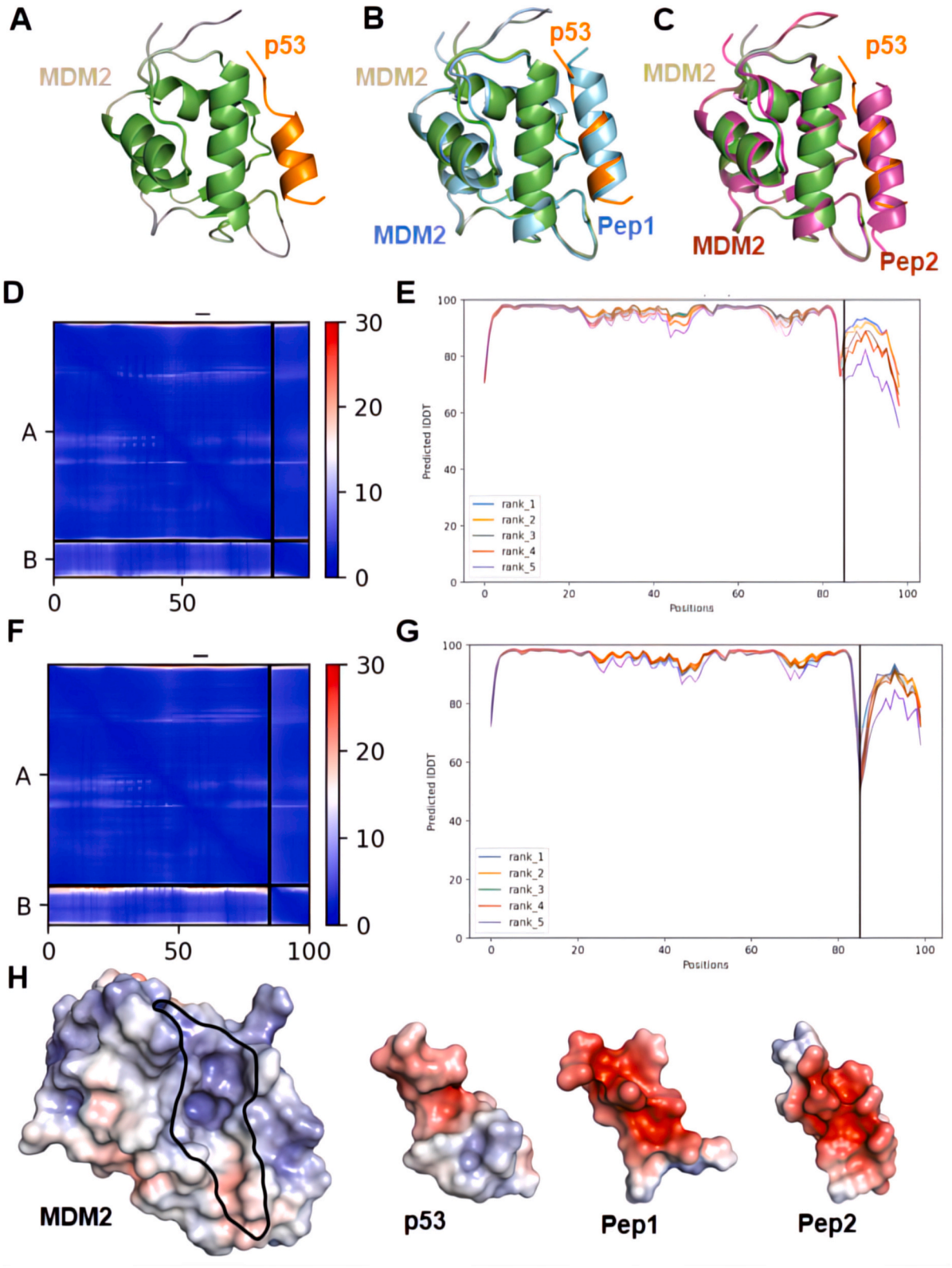

Fig. 1. Structural analysis of protein-peptide complexes. (A) Experimental structure of the MDM2-p53 complex as obtained from the protein data bank (PDB: 1YCR). (B) and (C) Superimposition of the predicted models of MDM2 in complex with Pep1 (cyan) and Pep2 (purple), respectively, over the experimental complex structure (green and orange coloration, respectively for MDM2 and p53). (D) and (E) Illustrations depicting the Positional Average Error (PAE) and predicted Local Distance Difference Test (pLDDT) for the three-dimensional structure of the MDM2-Pep1 complex, as predicted by Alphafold multimer. (F) and (G) Illustrations depicting the PAE and pLDDT for the three-dimensional structure of the MDM2-Pep2 complex, as predicted by Alphafold multimer. (H) Surface electrostatic potential of MDM2, p53, Pep1, and Pep2. The color-coded representations highlight regions of positive, negative, and neutral electrostatic potentials, visualized in blue, red, and white gradients, respectively. (For interpretation of the references to color in this figure legend, the reader is referred to the web version of this article.)

potential enhancement in the binding affinity of the designed peptide binders (Pep1 and Pep2) to MDM2. The nuanced electrostatic analysis thus contributes valuable insights into the molecular basis of their interaction and highlights the potential for increased binding efficacy in the designed peptide candidates (Fig. 1G).

3.3. Designed peptide binders exhibit improved predicted thermal stability

Diverse environmental factors can exert significant influence on the stability of proteins, and among these, thermal stability emerges as a crucial determinant [50]. The thermal stability of proteins holds particular importance as numerous essential biological processes unfold within a specific temperature range. Proteins exhibiting lower thermal stability are susceptible to aggregation at physiological temperatures, culminating in the loss of functional activity, dysfunctionality, or the formation of potentially harmful protein aggregates [27,51,52].

We delved into the estimation of the melting temperature for each of the peptides. This analysis revealed that the thermal stability of the designed peptide binders (Pep1 and Pep2), compared to the p53 peptide, improved slightly (Table 1) despite the observed increase in their negative electrostatic potentials (Fig. 1G). This predicted resilience in thermal stability is a promising characteristic, suggesting that the designed peptide binders have the potential to maintain their structural integrity despite their elevated negative electrostatic potentials. Such findings are crucial for understanding the robustness of these peptides under physiological conditions, indicating their potential utility as stable and effective molecular tools for targeted interactions with MDM2.

3.4. Pep1 and Pep2 display comparable in silico structural stability with p53 in complex with MDM2

The significance of employing MD simulation stems from the dynamic nature inherent in biomolecules, particularly proteins, which undergo essential motions for proper functionality. MD simulation offers a powerful tool for modeling the intricate flexibility and conformational changes exhibited by biomolecules at the atomic level—a feat challenging to achieve through experimental methods [53–56]. We conducted 1-microsecond simulations on each of the p53-, Pep1-, and Pep2-MDM2 complexes. Subsequently, we assessed the stability of these complexes by computing various post-simulation parameters, including RMSD (root mean square deviation), RMSF (root mean square fluctuation), Rg (radius of gyration), SASA (solvent accessible surface area), and PCA (principal component analysis) (Fig. 2). Additionally, our analysis extended to include the calculation of FEL (free energy landscapes) and kernel densities to elucidate the probability density function derived from our RMSD and Rg datasets (Supplementary Figs. S2–S4). This multifaceted approach provided a comprehensive understanding of the dynamic behavior and stability of the protein-peptide complexes under investigation.

The RMSD serves as a fundamental and primary parameter in the analysis of MD trajectories, playing a crucial role in assessing the stability and conformational changes of biomolecules [57,58]. We employed the RMSD to quantify the deviations between the backbones of the proteins, comparing their initial structural conformation to their final positions over the course of the MD simulations, as a way of evaluating the stability profile of each protein-peptide complex (Fig. 2A). The consistently low RMSD values across all complexes indicated a noteworthy level of stability, with the MDM2-Pep1 trajectory being the most stable among the complexes. Furthermore, this complex demonstrated a remarkable ability to maintain equilibrium throughout the entire simulation period.

The Root Mean Square Fluctuation (RMSF) is a valuable metric for comprehensively examining residue-wise fluctuations within a protein throughout its MD trajectory [59,60]. This parameter provides a detailed portrayal of the dynamic behavior of individual residues or domains within the protein, allowing for a nuanced understanding of their fluctuation patterns [61]. For each protein-peptide complex, we generated the RMSF plot, depicting RMSF (in nanometers) against residue number (Fig. 2B). Notably, the MDM2-Pep2 complex exhibited a discernible peak in fluctuation around residues 100–113 (Fig. 2B). Despite this localized heightened fluctuation, the RMSF profiles for all three complexes collectively indicated a general low degree of fluctuation across the entirety of the simulation period. This observation underscores the overall stability and controlled dynamics of the studied complexes.

For additional understanding of the stability profiles of the protein-peptide complexes, we conducted an analysis of the Rg and SASA (Fig. 2C and D). These parameters contribute valuable insights into the compactness and solvent interaction characteristics of the folded protein structures [62,63]. Conventionally, an ideal Rg value is lower for a globular folded state, indicating a tightly packed structure. In contrast, an expanded form or a protein with a higher number of loops and turns tends to exhibit a relatively higher Rg value [64]. Similarly, for proteins of the same size, a folded globular state typically corresponds to a lower SASA value, while an expanded form of the protein tends to show a higher SASA value [65]. Analysis of the Rg and SASA plots revealed consistently low gyration and solvent accessibility values across the trajectories of all three complexes (Fig. 2C and D). This observation aligns with the findings from our earlier analyses of the RMSD and RMSF plots, collectively suggesting a high degree of structural compactness within the studied complexes.

To conclude this phase of the study, we delved into an intricate analysis encompassing principal components, free energy landscapes, and probability density functions through kernel density estimation (Fig. 2E, Supplementary Figs. S2–S4). These advanced analytical methods were employed to unravel the collective motion of the protein-peptide complexes, decipher atomic fluctuations within their structures, glean insights into the energetics governing different conformational states in the MD trajectories, and ascertain the probability density distribution.

The principal component analysis provided a holistic view of the collective motion of the protein-peptide complexes, unveiling patterns of correlated atomic motions (Fig. 2E) [66]. This insightful approach shed light on the dynamic behavior of the complexes, facilitating the identification of concerted movements and their implications for structural stability (Fig. 2E). The exploration of free energy landscapes offered a nuanced understanding of the energetics governing diverse conformational states within the MD trajectories [67,68]. This analysis enabled us to discern the stability of different structural configuration of the complexes, providing valuable information on the energetically favored and less favorable states (Supplementary Fig. S2). The probability density function, assessed through kernel density estimation, provided a statistical representation of the distribution of atomic positions within the complexes. This comprehensive evaluation illuminated the likelihood of specific structural conformations, enriching our understanding of the dynamic interplay within the protein-peptide complexes (Supplementary Figs. S3 and S4). Collectively, the amalgamation of these post-simulation analyses including RMSD, RMSF, Rg, SASA, principal components, free energy landscapes, and probability density functions reinforces our broad conclusion that the three protein-peptide complexes consistently demonstrate high structural stability.

Table 1
Prediction of the whole-cell and cell lysate melting temperature (Tm) for p53 and the designed peptide binders.

Peptides	Cell (Tm ^{0}C)	Lysate (Tm ^{0}C)
p53	56.77	56.35
Pep1	58.72	58.54
Pep2	59.32	59.31

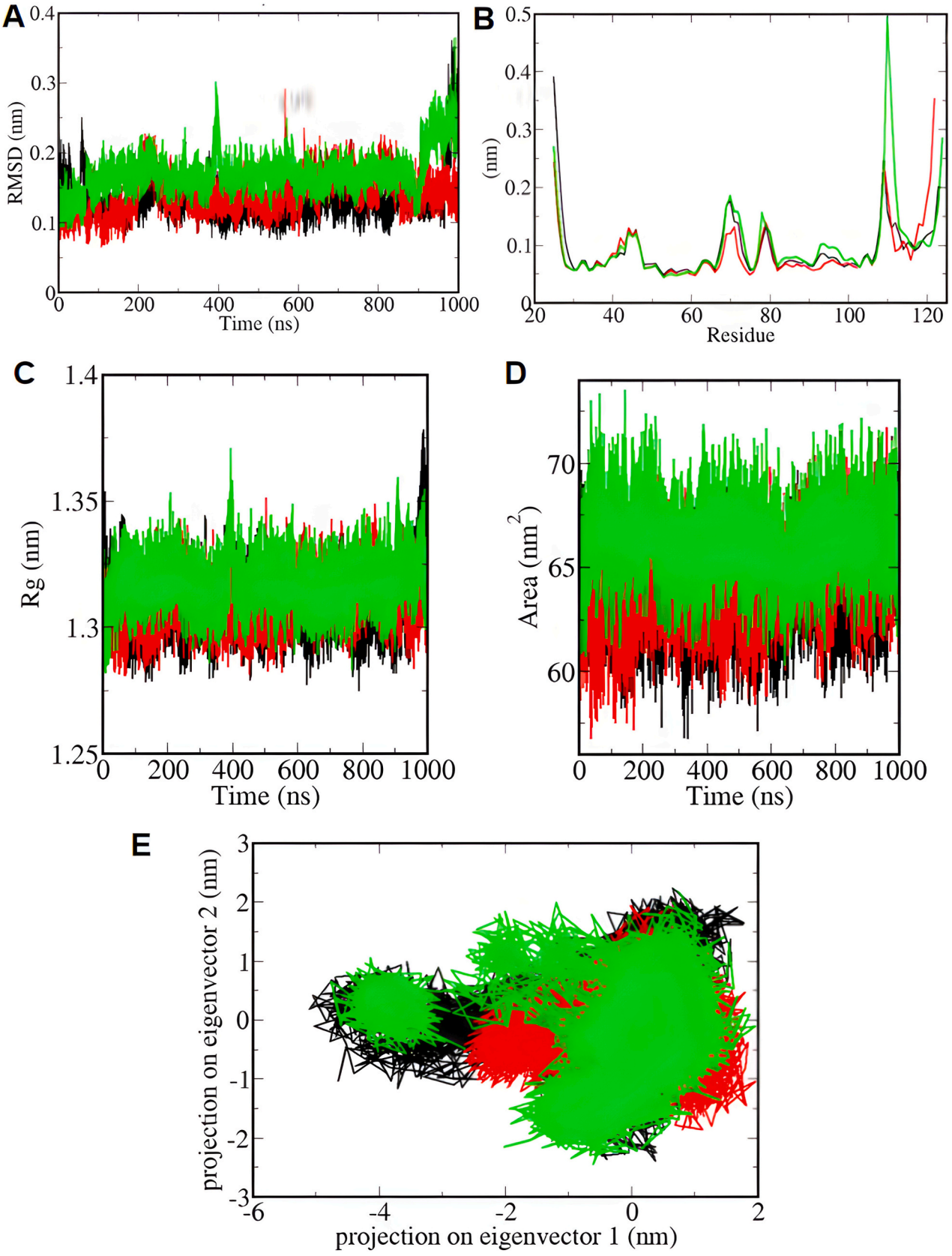

Fig. 2. Post-simulation analyses of protein-peptide complexes following the all-atom MD simulations. (A), (B), (C), (D), and (E) represent individual plots for the calculated RMSD, RMSF, Rg, SASA, and PCA, respectively. Trajectories of the complex of MDM2 with p53, Pep1, and Pep2 are shown in black, red, and green colors, respectively. (For interpretation of the references to color in this figure legend, the reader is referred to the web version of this article.)

3.5. Dissociation of the p53 and designed peptides from the MDM2 binding interface

To thoroughly investigate the binding and unbinding dynamics of MDM2 with the studied peptides (p53, Pep1, and Pep2), we conducted extensive steered MD simulations [69,70]. This approach allowed for a detailed examination of the intricate interactions governing the stability of the protein-peptide complexes. The low-energy structures obtained from the initial all-atom MD simulations served as the starting structures for the enhanced sampling simulations. Leveraging the CHAPERONg automation and analysis tool [26], we extracted the lowest energy structures representing the most stable conformations for each protein-peptide complex. These structures were identified from the free energy surface post-simulation calculations (Supplementary Fig. S2).

Our first SMD analysis focused on the structural dynamics of the MDM2-p53 complex, tracing its evolution from the starting configuration to the point of dissociation (Figs. 3 and 4; Supplementary Figs. S5 and S6; Supplementary movie 1). In the starting configuration, illustrated in Fig. 4A, a multitude of intermolecular interactions (including hydrogen bond interactions with GLY-58, GLN-72, TYR-104, hydrophobic interactions with LYS-51, ILE61, TYR-67, and salt bridge interaction with LYS-51) were evident between the bound p53 peptide and specific interface residues of MDM2. These interactions closely mirrored the structural features elucidated in the experimental MDM2-p53 complex by Kussie et al. [25] affirming the consistency of our computational model with experimental findings.

Notably, at 50 ps into the simulation, a significant portion of these intermolecular interactions persisted, indicating that the maximum pull force had not yet been achieved (Fig. 4A). However, around 100 ps into the pulling phase, a substantial number of the initially observed interactions had already been disrupted. Only the salt bridge interaction with LYS-51 and the hydrogen bond interaction with GLN-72 remained intact at this stage (Fig. 4A). The attainment of the maximum pull force, approximately 650 KJ/mol/nm (mean of three replica runs), occurred shortly thereafter, marking the point of complete dissociation of the protein-peptide interaction (Fig. 3A and D). By this time, p53 had been successfully pulled over a distance of 1.5 nm (Supplementary Figs. S5A and D, S6A and D). This detailed analysis provided a detailed understanding of the stepwise dissociation process, shedding light on the specific interactions that contribute to the stability and eventual disruption of the MDM2-p53 complex during the course of the simulation.

Next, we carried out a detailed structural analysis on the MDM2-Pep1 complex, examining its conformational changes from the initial configuration. Remarkably, Pep1 manifested distinct intermolecular interaction patterns with MDM2 interface residues, setting it apart from the p53 interactions. Noteworthy differences included Pep1's engagement in unique hydrogen bond, hydrophobic, and salt bridge interactions with specific residues of MDM2, diverging from the interaction profile observed with the p53 peptide (Fig. 4B). Although, hydrophobic interactions similar to those observed in the MDM2-p53 interaction were seen (with LYS-51 and TYR-67), Pep1 further demonstrated additional distinct interactions with MDM2 residues (Fig. 4A and B). At the 50 ps mark of the pulling simulation, numerous intermolecular interactions between Pep1 and MDM2 were sustained, echoing the observations made during the p53 pulling simulation. However, in contrast to the p53 scenario where only the last two interactions remained at 100 ps, Pep1 maintained several intermolecular interactions with MDM2 at this stage (Fig. 4B). This observation hinted at the requirement for additional pull force to achieve the complete dissociation of Pep1 from MDM2.

We further examined an additional snapshot at 150 ps of the pulling simulation (Fig. 4B) and found that the hydrogen bond with THR-26 of MDM2 was the only interaction remaining to be broken before the maximum pull force, estimated at approximately 800 KJ/mol/nm (Fig. 3B and D). Intriguingly, this occurred at a comparable displacement (1.5 nm) to that observed in the p53 pulling simulations (Supplementary Figs. S5B and D, S6B and D; Supplementary movie 2). This detailed structural analysis highlighted the differences in the dissociation dynamics between Pep1 and p53, providing a comprehensive understanding of their respective interactions with MDM2.

Next, we conducted a thorough analysis of the dissociation dynamics between Pep2 and MDM2. Interestingly, we observed a notable degree of similarity in intermolecular interactions between the starting configurations of MDM2 in complex with p53 and Pep2 (Fig. 4A and C). Similar to the pulling simulation of p53, Pep2 retained a substantial number of its starting configuration interactions at 50 ps (Fig. 4C). However, by 80 ps into the pulling phase, only the hydrogen bond interaction between Pep2 and the GLN-72 residue of MDM2 persisted among the initial conformation interactions (Fig. 4C).

Notably, a new interaction with the LYS-51 residue of MDM2 emerged at this stage, suggesting that these two interactions were the last to be disrupted before reaching the maximum pull force (Fig. 4C). This observation implied a distinctive dissociation pattern for Pep2 compared to p53 and Pep1. The pulling simulation for Pep2 required the lowest pull force, estimated at 600 KJ/mol/nm (Fig. 3C and D). Remarkably, this force was achieved at a similar displacement rate to that observed for p53 and Pep1 (Supplementary Figs. S5C and D, S6C and D; Supplementary movie 3). This detailed analysis sheds light on the specific interactions that govern the dissociation dynamics of Pep2 from MDM2, providing valuable insights into the unique features of this peptide's interaction with the target protein.

3.6. Umbrella sampling simulations suggest that Pep1 is a higher-affinity binder of MDM2 than p53 and Pep2

The determination of binding affinity in protein-peptide complexes holds paramount significance, as it serves as a pivotal parameter governing protein interactions and delineates the structure-activity relationships that underlie essential biological processes [71,72]. The precise measurement of binding affinity is instrumental in unraveling intricate biochemical pathways and deciphering protein interaction networks. Additionally, it plays a vital role in drug design and discovery, contributing to the enhancement of drug specificity [71,72]. Following the SMD simulations, we employed the umbrella sampling simulation approach to estimate the binding affinity of the peptides for MDM2 (Fig. 5; Supplementary Figs. S7–S9).

The configurations derived from the SMD simulations trajectory were used to create the umbrella sampling windows featuring a center of mass spacing of 0.2 nm along the reaction coordinates (Fig. 5; Supplementary Figs. S7–S9). For the binding and unbinding dynamics of each protein-peptide complexes, the binding free energies ($\Delta G_{binding}$) were determined by assessing the net change in the Gibbs free energy (G) during the transition from the bound state of each peptide to their unbound state from the MDM2 binding pocket (Fig. 5, Table 2). Similar to the SMD simulations conducted earlier, the umbrella sampling simulations were also performed in three independent replica runs, and the average of each was considered for our binding affinity estimation.

Upon careful examination of the potential of mean force plots (Fig. 5) and the computed averages of the binding free energies (Table 2), it becomes evident that Pep1 demonstrates a notably higher binding affinity toward MDM2 compared to p53 and Pep2. This observation, consistent with the SMD results (Figs. 3 and 4; Supplementary Figs. S5 and S6), suggests Pep1 as potential inhibitor of the MDM2-p53 interaction, positioning it as a promising candidate for further experimental investigation as an anticancer agent targeting the MDM2-p53 interactions.

4. Conclusion

This study focused on the strategic design of peptide binders targeting the MDM2-p53 interface, utilizing advanced protein design

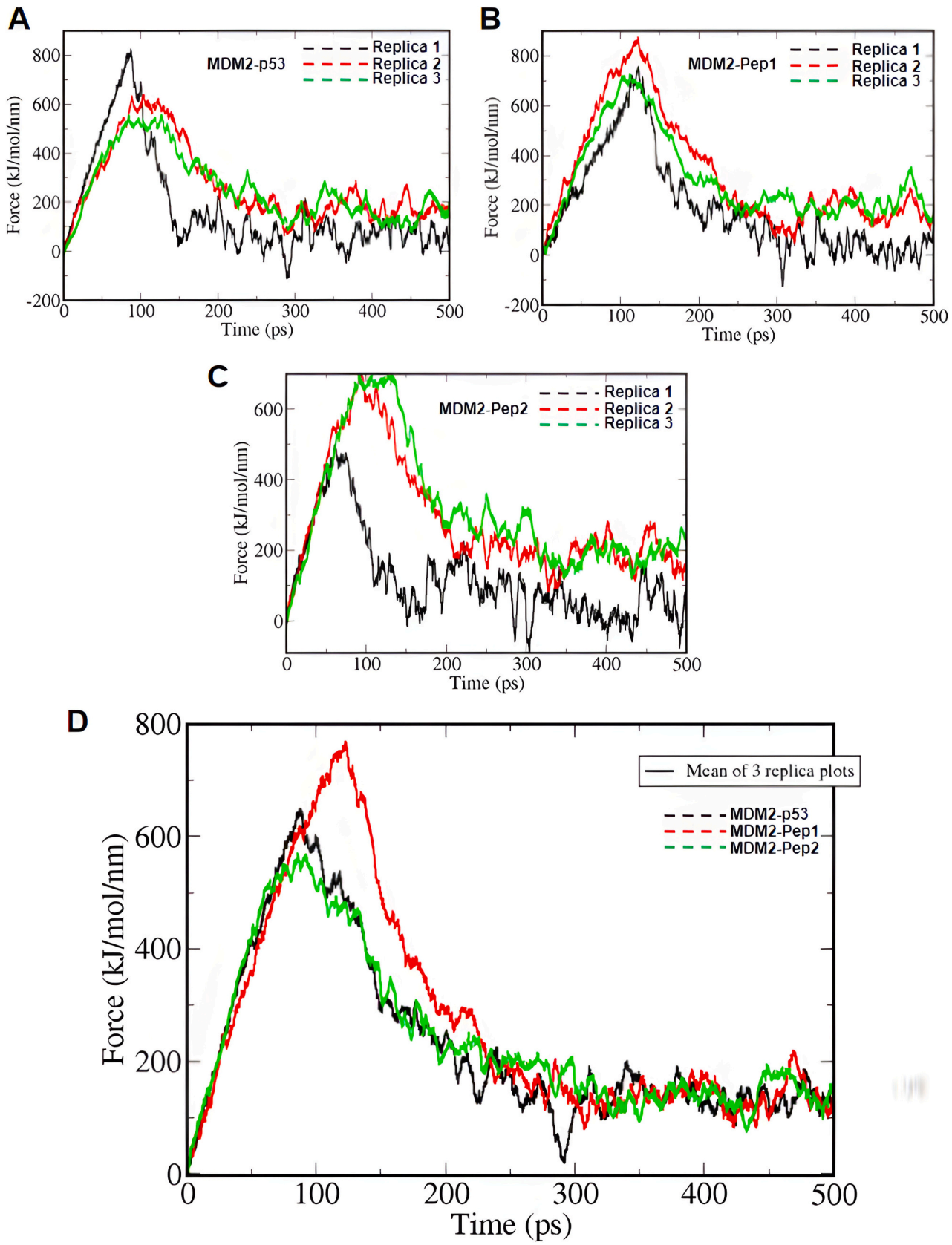

Fig. 3. Center of mass pulling of the protein-peptide complexes. (A), (B), and (C) show the COM trajectories for the pulling of p53, Pep1, and Pep2, respectively. Because the simulations were performed in three replica runs, trajectories for the 1st, 2nd, and 3rd runs are shown in black, red, and green colors, respectively. (D) COM trajectories for the mean of the three replica plots. The mean of the replica simulations for the pulling of p53, Pep1, and Pep2 are shown in black, red, and green colors, respectively. (For interpretation of the references to color in this figure legend, the reader is referred to the web version of this article.)

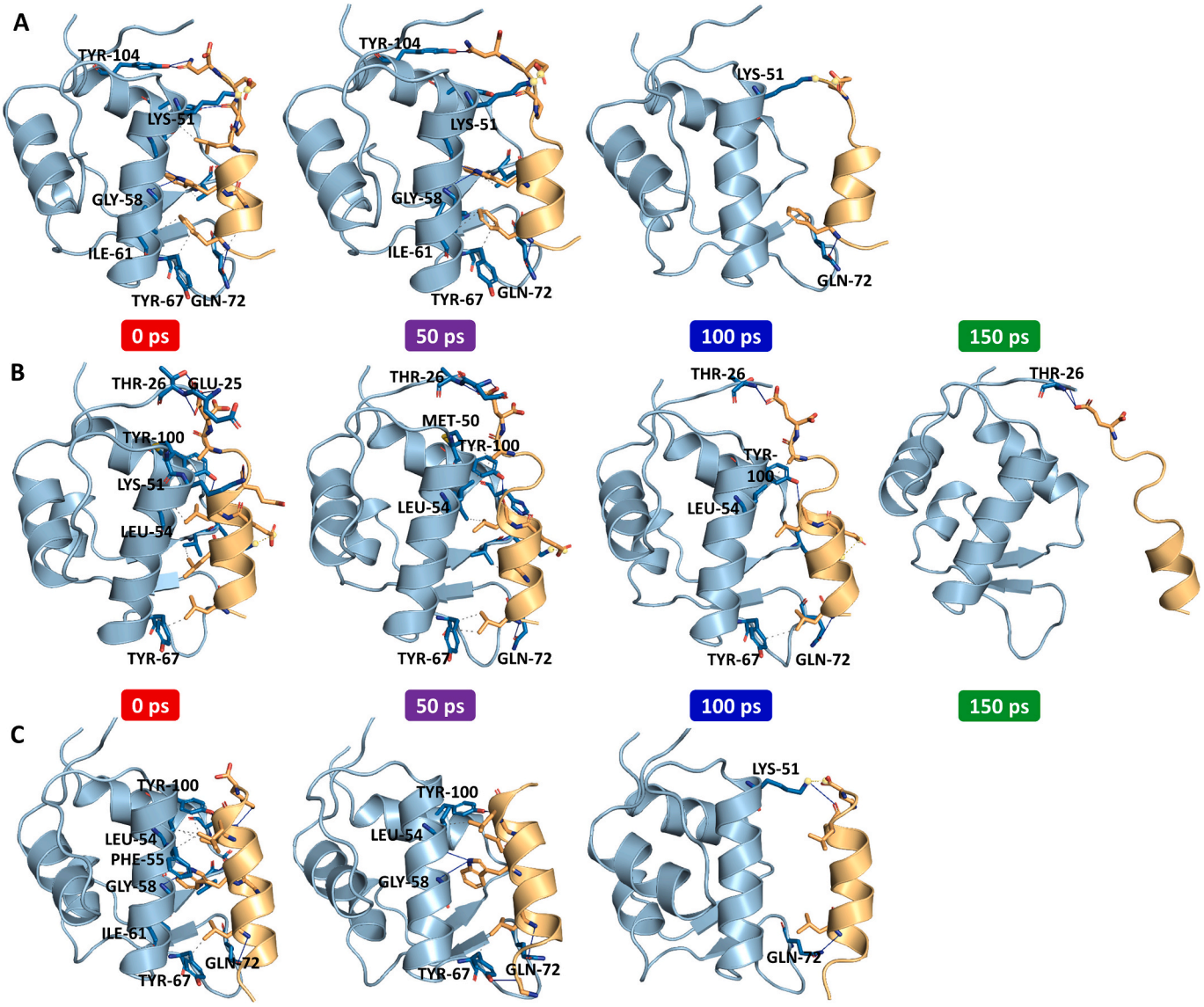

Fig. 4. Unbinding of p53, Pep1, and Pep2 from MDM2. (A), (B), and (C) display snapshots of representative configurations during the dissociation of p53 from MDM2 at 0, 50, 100, and 150 ps, respectively. MDM2 and its interacting peptides (p53, Pep1, and Pep2) are shown in blue and brown cartoons, respectively while their surface interactions are represented in sticks. (For interpretation of the references to color in this figure legend, the reader is referred to the web version of this article.)

methodologies in combination with comprehensive all-atom and enhanced sampling molecular dynamics simulations. These approaches included RFdiffusion, which provided generative models for protein backbones, ProteinMPNN for *in silico* design of amino acid sequences on given backbones, and AlphaFold structure predictions for the refinement and selection of candidate peptides. Notably, two peptides, Pep1 and Pep2, were identified as potential MDM2 binders. Electrostatic complementarity analysis was conducted, revealing an enhanced negative potential in Pep1 and Pep2, indicative of an increased binding affinity to MDM2. Remarkably, the designed peptides are predicted to maintain thermal stability, a crucial factor for functional competence under physiological conditions. Molecular dynamics simulations provided comprehensive insights into the stability, fluctuation, and structural dynamics of the protein-peptide complexes while the dissociation dynamics highlighted unique interactions governing the unbinding of p53, Pep1, and Pep2 from the MDM2 binding interface. Umbrella sampling simulations estimated binding affinities, revealing Pep1 as a higher-affinity MDM2 binder compared to p53 and Pep2. This suggests Pep1 as a potential inhibitor of MDM2-p53 interactions, emphasizing its candidacy for anticancer therapeutics. Future studies could focus on experimental validation of the designed peptides and their functional implications. Additionally, the identified peptide binders may serve as starting points for drug development efforts, and further optimization and refinement could enhance their therapeutic potential.

Supplementary data to this article can be found online at https://doi.org/10.1016/j.ijbiomac.2024.131840.

CRediT authorship contribution statement

Olanrewaju Ayodeji Durojaye: Writing – original draft, Visualization, Methodology, Formal analysis, Conceptualization. **Abeeb Abiodun Yekeen:** Writing – review & editing, Visualization, Validation, Software, Formal analysis. **Mukhtar Oluwaseun Idris:** Validation, Investigation, Data curation. **Nkwachukwu Oziamara Okoro:** Validation, Investigation, Data curation. **Arome Solomon Odiba:** Supervision, Project administration, Conceptualization. **Bennett Chima Nwanguma:** Supervision, Project administration, Conceptualization.

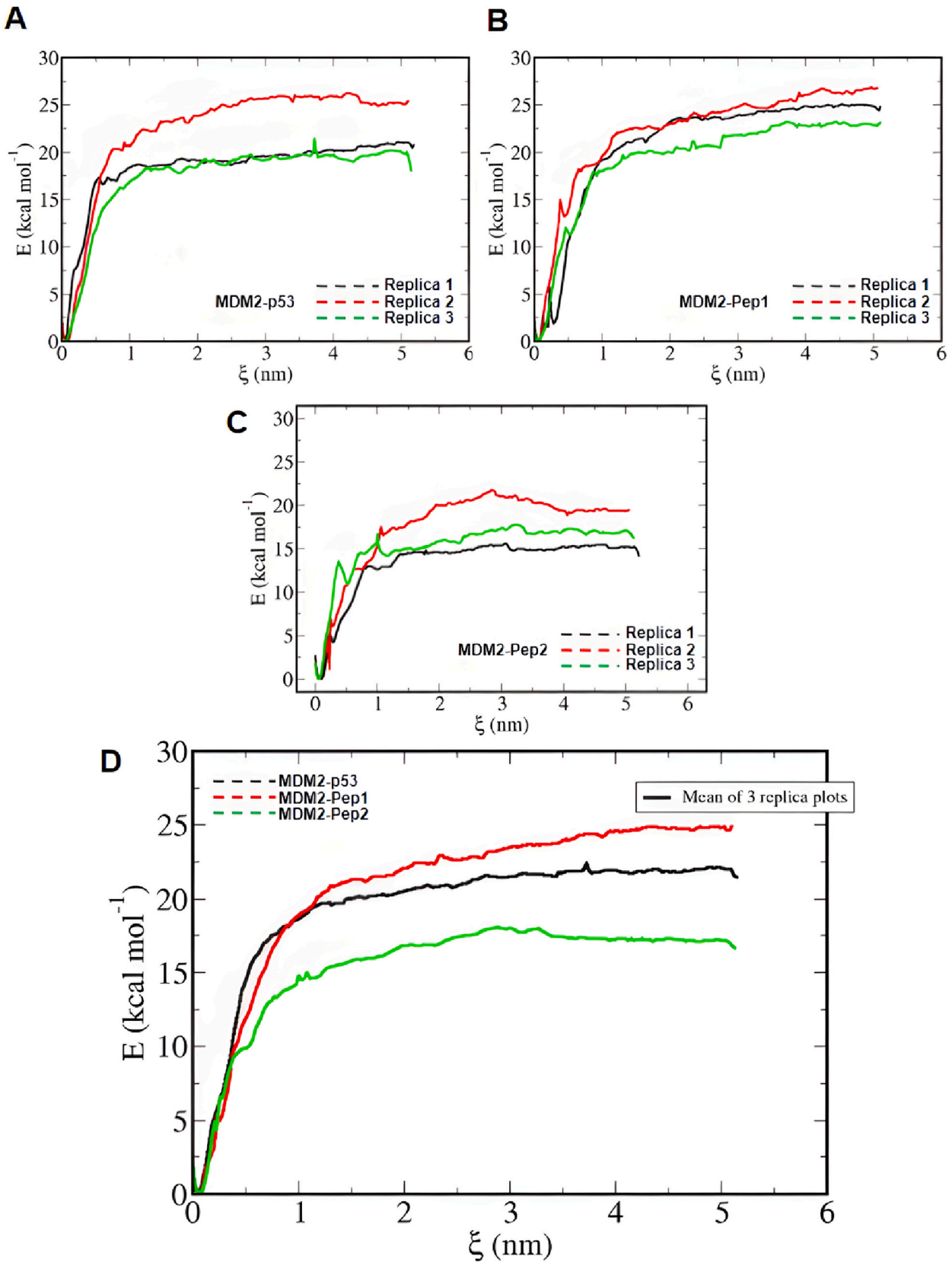

Fig. 5. Estimation of binding free energy using the Weighted Histogram Analysis Method. (A), (B), and (C) show the pull mean force (PMF) trajectories for the binding energy estimation of MDM2 in complex with p53, Pep1, and Pep2, respectively. Because the umbrella sampling simulations were performed in three replica runs, trajectories for the 1st, 2nd, and 3rd runs are shown in black, red, and green colors, respectively. (D) PMF trajectories for the mean of the three replica plots. The mean of the three replica umbrella sampling simulations for the $\Delta G_{binding}$ of p53, Pep1, and Pep2 I complex with MDM2 are shown in black, red, and green colors, respectively. (For interpretation of the references to color in this figure legend, the reader is referred to the web version of this article.)

Table 2
Binding free energy calculation of the protein-peptide complexes.

Protein-peptide complexes	Binding free energy (Kcal/mol)			
	Replica 1	Replica 2	Replica 3	Average
MDM2-p53	−16.84	−26.23	−21.43	−21.50 ± 3.83
MDM2-Pep1	−24.25	−26.82	−23.22	−24.76 ± 1.51
MDM2-Pep2	−14.21	−21.79	−17.79	−17.93 ± 3.09

Declaration of competing interest

None declared.

Acknowledgement

I would like to extend my heartfelt appreciation to my co-authors, whose invaluable contributions have been instrumental in the success of this project. Their dedication, expertise, and collaborative spirit have enriched our research endeavors and facilitated the achievement of our goals.

I am deeply grateful to the CAS-TWAS (Chinese Academy of Sciences and The World Academy of Sciences) for awarding me a full scholarship to support my doctoral program at the University of Science and Technology of China. This generous support has enabled me to pursue my academic aspirations and has been integral to my professional development. Additionally, I wish to express my sincere gratitude to the developers of the Tamarind Bio platform, Sherry and Deniz, for graciously providing access to their state-of-the-art computational tools. Their innovative platform has greatly enhanced the scope and depth of our research capabilities, contributing significantly to the quality of our work.

Lastly, I would like to acknowledge and appreciate my fellow executives of the Nigerians in Diaspora Organization (NiDO East China), under the exemplary leadership of Mr. Edwards Nathaniel Osas. Their unwavering support, encouragement, and tireless efforts in serving the Nigerian community in East China have been a source of inspiration and motivation throughout my academic journey.

References

[1] L. Lang, A. Perez, Binding ensembles of p53-MDM2 peptide inhibitors by combining bayesian inference and atomistic simulations, Molecules 26 (1) (2021) 198.
[2] V.B. Sulimov, D.C. Kutov, A.V. Sulimov, Advances in docking, Curr. Med. Chem. 26 (42) (2019) 7555–7580.
[3] S. Cosmas, et al., Comparative in-silico parmacokinetics and molecular docking study on gedunin isolated from Azadirachta indica, its modified derivatives and selected antifolate drugs as potential dihydrofolate reductase inhibitors of Plasmodium falciparum, Int. J. Comput. Biol. Drug Des. 13 (3) (2020) 237–254.
[4] A.S. Oluwaseun, et al., Identification of lead inhibitors of TMPRSS2 isoform 1 of SARS-CoV-2 target using neural network, random forest, and molecular docking, in: Data Science for COVID-19, Elsevier, 2022, pp. 547–575.
[5] G. Weng, et al., Comprehensive evaluation of fourteen docking programs on protein–peptide complexes, J. Chem. Theory Comput. 16 (6) (2020) 3959–3969.
[6] P. Agrawal, et al., Benchmarking of different molecular docking methods for protein-peptide docking, BMC Bioinformatics 19 (13) (2019) 105–124.
[7] P. Zhou, et al., HPEPDOCK: a web server for blind peptide–protein docking based on a hierarchical algorithm, Nucleic Acids Res. 46 (W1) (2018) W443–W450.
[8] G.O. Ibiang, et al., Oral cavity infection by the SARS-CoV-2: emphasizing the essence of masking and peptide therapeutics, Egyptian Journal of Medical Human Genetics 23 (1) (2022) 1–7.
[9] P. Zhou, et al., Hierarchical flexible peptide docking by conformer generation and ensemble docking of peptides, J. Chem. Inf. Model. 58 (6) (2018) 1292–1302.
[10] S.-Y. Huang, Exploring the potential of global protein–protein docking: an overview and critical assessment of current programs for automatic ab initio docking, Drug Discov. Today 20 (8) (2015) 969–977.
[11] D.S. Paul, P. Karthe, Improved docking of peptides and small molecules in iMOLSDOCK, J. Mol. Model. 29 (1) (2023) 12.
[12] D. Soler, Y. Westermaier, R. Soliva, Extensive benchmark of rDock as a peptide-protein docking tool, J. Comput. Aided Mol. Des. 33 (7) (2019) 613–626.
[13] Y. Zhang, M.F. Sanner, AutoDock CrankPep: combining folding and docking to predict protein–peptide complexes, Bioinformatics 35 (24) (2019) 5121–5127.
[14] S.V. Torres, et al., De novo design of high-affinity binders of bioactive helical peptides, Nature (2023) 1–3.
[15] N.R. Bennett, et al., Improving de novo protein binder design with deep learning, Nat. Commun. 14 (1) (2023) 2625.
[16] L. Cao, et al., Design of protein-binding proteins from the target structure alone, Nature 605 (7910) (2022) 551–560.
[17] T. Zhou, et al., Molecular mechanism of CCDC106 regulating the p53-Mdm2/MdmX signaling axis, Sci. Rep. 13 (1) (2023) 21892.
[18] M. Pazgier, et al., Structural basis for high-affinity peptide inhibition of p53 interactions with MDM2 and MDMX, Proc. Natl. Acad. Sci. 106 (12) (2009) 4665–4670.
[19] X. Xie, et al., Recent advances in targeting the "undruggable" proteins: from drug discovery to clinical trials, Signal Transduct. Target. Ther. 8 (1) (2023) 335.
[20] A. Carrera-Aubesart, et al., Topoisomeric membrane-active peptides: a review of the last two decades, Pharmaceutics 15 (10) (2023) 2451.
[21] K. Somasundaram, W.S. El-Deiry, Tumor suppressor p53: regulation and function, Front. Biosci. 5 (5) (2000) D424–D437.
[22] D.G. Kirsch, M.B. Kastan, Tumor-suppressor p53: implications for tumor development and prognosis, J. Clin. Oncol. 16 (9) (1998) 3158–3168.
[23] K. Yoshida, Y. Miki, The cell death machinery governed by the p53 tumor suppressor in response to DNA damage, Cancer Sci. 101 (4) (2010) 831–835.
[24] C.A. Mendoza Rodríguez, M.A. Cerbón, El gen supresor de tumores p53: mecanismos de acción en la proliferación y muerte celular, Rev. Invest. Clín (2001) 266–273.
[25] P.H. Kussie, et al., Structure of the MDM2 oncoprotein bound to the p53 tumor suppressor transactivation domain, Science 274 (5289) (1996) 948–953.
[26] A.A. Yekeen, O.A. Durojaye, M.O. Idris, H.F. Muritala, R.O. Arise, CHAPERONg: A tool for automated GROMACS-based molecular dynamics simulations and trajectory analyses, Comput. Struct. Biotechnol. J. 28 (21) (2023) 4849–4858.
[27] F. Jung, et al., DeepSTABp: a deep learning approach for the prediction of thermal protein stability, Int. J. Mol. Sci. 24 (8) (2023) 7444.
[28] J.L. Watson, et al., De novo design of protein structure and function with RFdiffusion, Nature 620 (7976) (2023) 1089–1100.
[29] Tamarind Bio, State of the Art Computational Tools for Biology, Available from: https://www.tamarind.bio/, 2023.
[30] J. Dauparas, et al., Robust deep learning–based protein sequence design using ProteinMPNN, Science 378 (6615) (2022) 49–56.
[31] R. Evans, et al., Protein complex prediction with AlphaFold-Multimer, biorxiv (2021), p. 2021.10. 04.463034. (Preprint).
[32] M. Mirdita, et al., ColabFold: making protein folding accessible to all, Nat. Methods 19 (6) (2022) 679–682.
[33] J. Jumper, et al., Highly accurate protein structure prediction with AlphaFold, Nature 596 (7873) (2021) 583–589.
[34] W. Zheng, et al., Improving deep learning protein monomer and complex structure prediction using DeepMSA2 with huge metagenomics data, Nat. Methods (2024) 1–11.
[35] S. Unni, et al., Web servers and services for electrostatics calculations with APBS and PDB2PQR, J. Comput. Chem. 32 (7) (2011) 1488–1491.
[36] M.J. Abraham, et al., GROMACS: high performance molecular simulations through multi-level parallelism from laptops to supercomputers, SoftwareX 1 (2015) 19–25.
[37] E.F. Pettersen, et al., UCSF Chimera—a visualization system for exploratory research and analysis, J. Comput. Chem. 25 (13) (2004) 1605–1612.
[38] J. Huang, et al., CHARMM36m: an improved force field for folded and intrinsically disordered proteins, Nat. Methods 14 (1) (2017) 71–73.
[39] D.J. Evans, B.L. Holian, The nose–hoover thermostat, J. Chem. Phys. 83 (8) (1985) 4069–4074.
[40] V. Rühle, Pressure coupling/barostats, Journal Club (2008) 1–5.
[41] T. Darden, D. York, L. Pedersen, Particle mesh Ewald: an N·log (N) method for Ewald sums in large systems, J. Chem. Phys. 98 (12) (1993) 10089–10092.
[42] B. Hess, et al., LINCS: a linear constraint solver for molecular simulations, J. Comput. Chem. 18 (12) (1997) 1463–1472.
[43] P. Turner, XMGRACE, *Version 5.1. 19.* Center for Coastal and Land-Margin Research, Oregon Graduate Institute of Science and Technology, Beaverton, OR, 2005, p. 2.
[44] S. Kumar, et al., The weighted histogram analysis method for free-energy calculations on biomolecules. I. The method, J. Comput. Chem. 13 (8) (1992) 1011–1021.
[45] J.L. Watson, et al., Broadly applicable and accurate protein design by integrating structure prediction networks and diffusion generative models, BioRxiv (2022), p. 2022.12. 09.519842. (Preprint).
[46] V.J. Hoerschinger, et al., PEP-patch: electrostatics in protein–protein recognition, specificity, and antibody developability, J. Chem. Inf. Model. 63 (22) (2023) 6964–6971.
[47] A.J. McCoy, V.C. Epa, P.M. Colman, Electrostatic complementarity at protein/protein interfaces, J. Mol. Biol. 268 (2) (1997) 570–584.
[48] G. Grassmann, et al., Electrostatic complementarity at the interface drives transient protein-protein interactions, Sci. Rep. 13 (1) (2023) 10207.
[49] F. Vascon, et al., Protein electrostatics: from computational and structural analysis to discovery of functional fingerprints and biotechnological design, Comput. Struct. Biotechnol. J. 18 (2020) 1774–1789.
[50] O.A. Durojaye, Intracellular proteome compartmentalization: a biotin ligase-based proximity labeling approach, Cell Biosci. 11 (1) (2021) 165.
[51] C.-W. Chen, et al., iStable 2.0: predicting protein thermal stability changes by integrating various characteristic modules, Comput. Struct. Biotechnol. J. 18 (2020) 622–630.
[52] I. Pudžiuvelytė, et al., TemStaPro: protein thermostability prediction using sequence representations from protein language models, bioRxiv (2023), p. 2023.03. 27.534365. (Preprint).

[53] S. Sinha, B. Tam, S.M. Wang, Applications of molecular dynamics simulation in protein study, Membranes 12 (9) (2022) 844.
[54] O.A. Durojaye, Delineation of the CENP-LN sub-complex dissociation mechanism upon multisite phosphorylation during mitosis, J. Biomol. Struct. Dyn. (2023) 1–19.
[55] X. Wu, et al., Application of molecular dynamics simulation in biomedicine, Chem. Biol. Drug Des. 99 (5) (2022) 789–800.
[56] J.A. McCammon, B.R. Gelin, M. Karplus, Dynamics of folded proteins, nature 267 (5612) (1977) 585–590.
[57] A.S. Odiba, et al., A new variant of mutational and polymorphic signatures in the ERG11 gene of fluconazole-resistant Candida albicans, Infection and Drug Resistance 15 (2022) 3111.
[58] O.A. Durojaye, et al., Csc01 shows promise as a potential inhibitor of the oncogenic G13D mutant of KRAS: an in silico approach, Amino Acids 55 (12) (2023) 1745–1764.
[59] O.A. Durojaye, et al., MasitinibL shows promise as a drug-like analog of masitinib that elicits comparable SARS-Cov-2 3CLpro inhibition with low kinase preference, Sci. Rep. 13 (1) (2023) 6972.
[60] H.O. Uzoeto, et al., Computer-aided molecular modeling and structural analysis of the human centromere protein–HIKM complex, Beni-Suef University Journal of Basic and Applied Sciences 11 (1) (2022) 1–18.
[61] O.A. Durojaye, et al., Identification of a potential mRNA-based vaccine candidate against the SARS-CoV-2 spike glycoprotein: a reverse vaccinology approach, ChemistrySelect 7 (7) (2022) e202103903.
[62] R. Shukla, T. Tripathi, Molecular dynamics simulation of protein and protein–ligand complexes, in: Computer-Aided Drug Design, Springer, 2020, pp. 133–161.
[63] M.O. Idris, et al., Computer-aided screening for potential TMPRSS2 inhibitors: a combination of pharmacophore modeling, molecular docking and molecular dynamics simulation approaches, Journal of Biomolecular Structure and Dynamics 39 (15) (2021) 5638–5656.
[64] Y. Mazola, et al., A comparative molecular dynamics study of thermophilic and mesophilic β-fructosidase enzymes, J. Mol. Model. 21 (9) (2015) 1–11.
[65] R. Shukla, H. Shukla, T. Tripathi, Activity loss by H46A mutation in Mycobacterium tuberculosis isocitrate lyase is due to decrease in structural plasticity and collective motions of the active site, Tuberculosis 108 (2018) 143–150.
[66] C.C. David, D.J. Jacobs, Principal component analysis: a method for determining the essential dynamics of proteins, in: Protein Dynamics, Springer, 2014, pp. 193–226.
[67] E. Papaleo, et al., Free-energy landscape, principal component analysis, and structural clustering to identify representative conformations from molecular dynamics simulations: the myoglobin case, J. Mol. Graph. Model. 27 (8) (2009) 889–899.
[68] I. Tavernelli, S. Cotesta, E.E. Di Iorio, Protein dynamics, thermal stability, and free-energy landscapes: a molecular dynamics investigation, Biophys. J. 85 (4) (2003) 2641–2649.
[69] T. Banerjee, et al., Examining sialic acid derivatives as potential inhibitors of SARS-CoV-2 spike protein receptor binding domain, Journal of Biomolecular Structure and Dynamics (2023) 1–17.
[70] A. Volkova, P. Semenyuk, Tyrosine phosphorylation of recombinant hirudin increases affinity to thrombin and antithrombotic activity, Proteins 92 (3) (2024) 329–342.
[71] W.A. Abbasi, et al., ISLAND: in-silico proteins binding affinity prediction using sequence information, BioData Mining 13 (1) (2020) 1–13.
[72] J.A. Lemkul, D.R. Bevan, Assessing the stability of Alzheimer's amyloid protofibrils using molecular dynamics, J. Phys. Chem. B. 114 (4) (2010) 1652–1660.